5. THE ARCTIC—J. Richter-Menge, Ed.

a. Overview—J. Richter-Menge

The permanent presence of sea ice, ice sheets and continuous permafrost are defining features of the polar regions. The Arctic is further distinguished because it sustains a human population in a harsh environment. In this chapter we highlight observations that indicate changes and trends in the state of the physical components of the Arctic system, including the atmosphere, ocean, sea ice cover, land, and Greenland. In 2009 there continued to be widespread evidence of the impact of a general, Arctic-wide warming trend in surface air temperatures over land, evident since the mid-1960s. Significant regional and temporal variability was also widely apparent, tempering the dramatic evidence of warming reported in recent years (e.g., a record positive surface air temperature anomaly in 2008, record summer sea ice minimum extent in 2007, and record ocean surface temperature anomalies in 2007).

Surface temperature anomalies (relative to a 1961–90 reference period) highlight the major feature of current Arctic conditions: an Arctic amplification of temperature anomaly of a factor of two or more, relative to more southerly latitudes. Below normal precipitation (with reference to the 1971–2000 base period) led the Greenland ice sheet surface mass balance in 2009 to be 25% to 50% less positive than normal, despite below-normal melting and runoff across much of the ice sheet below ~1800 m altitude. The 34 widest marine-terminating glaciers in Greenland lost 101 km^2 ice area in 2009, within a remarkably linear ($R = -0.99$) annual loss rate of -106 km^2 over the past decade. The 2008/09 Arctic snow-cover season marked a continuation of relatively shorter snow seasons, due primarily to an early disappearance of snow cover in spring. Observations show a general increase in permafrost temperatures during the last several decades in Alaska, northwest Canada, Siberia, and Northern Europe. Changes in the timing of tundra green up and senescence are also occurring, with earlier green up in the High Arctic and a shift to a longer green season in fall in the Low Arctic. The 2009 summer minimum sea ice extent was the third-lowest recorded since 1979. Surface ocean temperatures remained relatively warm and surface water was much fresher than in the 1970s.

Linkages between the various elements of the Arctic systems continue to emerge. For instance, tendencies in the magnitude and distribution of upper ocean temperatures are observed to be strongly dependent on changes in the characteristics (e.g., pace and location) of the summer sea ice retreat and their effect on local atmospheric warming. The heat accumulated in the surface and near-surface layers of the ocean during the summer is then released back to the atmosphere in the following autumn, impacting temperatures in the lower troposphere. The coupling between the atmosphere, ocean, and sea ice has also impacted the overall characteristics of the Arctic sea ice cover, which is now dominated by relatively thin seasonal ice. The effects of the retreating sea ice also influence the temperature and vegetation of adjacent lands. Temporal analyses generally show that, within a specific region, periods of lower sea ice concentration are correlated with warmer land surface temperatures and an increase in the amount of live green vegetation in the summer. In the Eurasian river drainage basins, the correlation between river discharge and sea ice extent, over the period 1979–2008, is greater than the correlation between precipitation and runoff.

b. Atmosphere—J. Overland, M. Wang, and J. Walsh

The annual mean temperature for 2009 over Arctic land areas was cooler than in recent years, although the average temperature for the last decade remained the warmest in the record beginning in 1900 (Fig. 5.1). The 2009 average was dominated by very cold temperatures in Eurasia in February (the coldest of the decade) and December, while the remainder of the Arctic remained warm (Fig. 5.2). The spatial distribution of annual temperature anomalies for 2009 has a

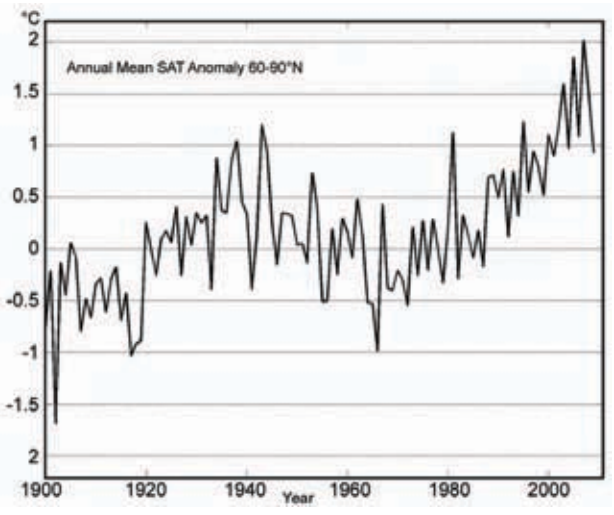

Fig. 5.1. Arctic-wide annual average surface air temperature anomalies relative to the 1961–90 mean, based on land stations north of 60°N from the CRUTEM 3v dataset, available online at www.cru.uea.ac.uk/cru/data/temperature/. Note this curve does not include marine observations.

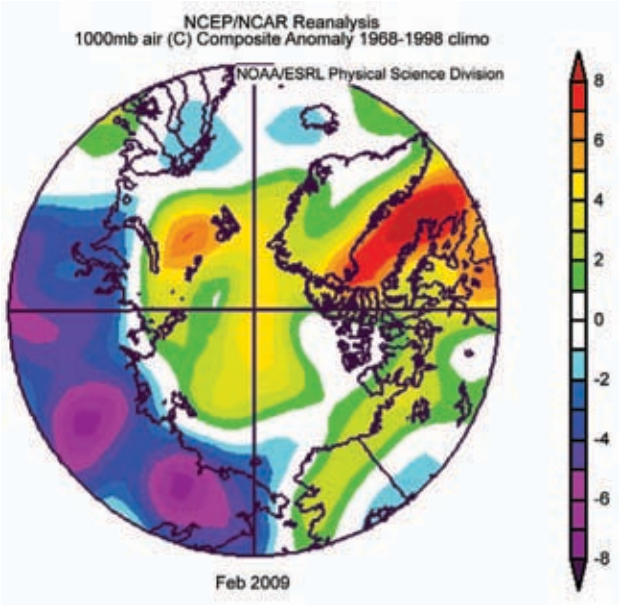

Fig. 5.2. Near-surface (1000 mb) air temperature in °C anomalies for February 2009. Anomalies are relative to the 1968–96 mean, according to the NCEP–NCAR reanalysis through the NOAA/Earth Systems Research Laboratory, generated online at www.cdc.noaa.gov.

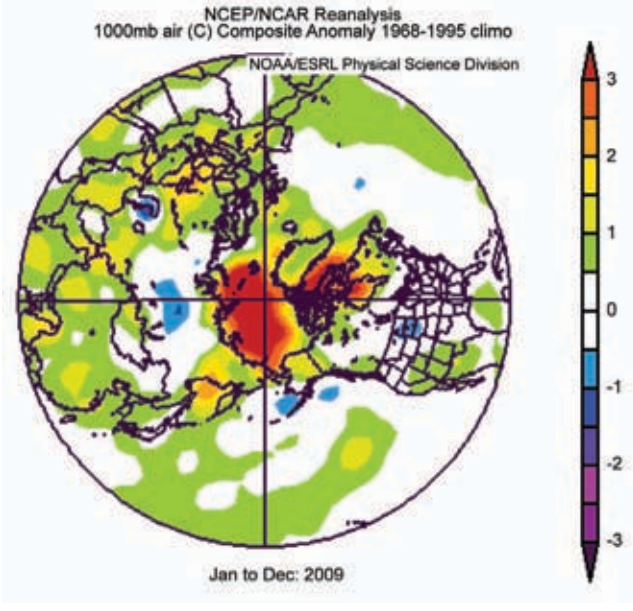

Fig. 5.3. Near-surface (1000 mb) annual air temperature in °C anomalies for 2009 over the Northern Hemisphere relative to 1968–96 mean according to the NCEP–NCAR reanalysis through the NOAA/Earth Systems Research Laboratory, generated online at www.cdc.noaa.gov. Arctic amplification of air temperature anomalies are a factor of two or more relative to lower latitudes.

pattern with values greater than 2.0°C throughout the Arctic, relative to a 1968–96 reference period (Fig. 5.3). These anomalies show the major feature of current Arctic conditions: a factor of two (or more) amplification of temperature relative to lower latitudes.

As noted in the Arctic sea ice section, September 2009 had the third minimum sea ice extent relative to the period when observations began in 1979. Although 2009 did not have a record sea ice minimum

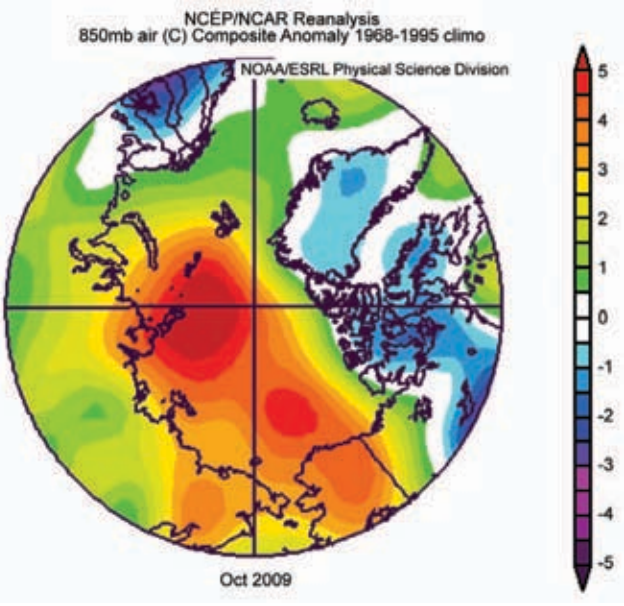

Fig. 5.4. Lower tropospheric (850 hPa) air temperature in °C anomalies for October 2009 relative to the 1968–96 mean according to the NCEP–NCAR reanalysis through the NOAA/Earth Systems Research Laboratory, generated online at www.cdc.noaa.gov.

in September, there were still extensive regions of open water in the Chukchi, East Siberian Laptev, and Kara Seas (see sea ice section below, Fig. 5.11), which allowed extra solar and longwave radiation to be absorbed by the ocean (see ocean section below, Fig. 5.5). This heat can be released back to the atmosphere the following autumn. This release of heat impacted temperatures in the lower troposphere (Fig. 5.4) with consequences for regional and far field wind patterns through horizontal gradients in the 500–1000 hPa thickness fields (Overland and Wang 2010).

The year 2009 ended with record-setting negative values for the Arctic Oscillation (AO) index, a condition favoring meridional (north–south) atmospheric flow. Thus, December 2009 and early 2010 exhibited extremes in both warm and cold temperatures with record-setting snow across lower latitudes. Northern Eurasia (north of 50° latitude to the Arctic coast)

and North America (south of 55° latitude) were particularly cold (monthly anomalies of –2°C to –10°C). Arctic regions had anomalies of +4°C to +12°C. While individual weather events cannot be directly linked to larger scale climate changes, recent data analysis and modeling suggest a link between loss of sea ice and a shift to an increased impact from the Arctic on midlatitude climate (Francis et al. 2009; Honda et al. 2009).

c. Ocean—A. Proshutinsky, M.-L. Timmermans, I. Ashik, A. Beszczynska-Moeller, E. Carmack, I. Frolov, R. Krishfield, F. McLaughlin, J. Morison, I. Polyakov, K. Shimada, V. Sokolov, M. Steele, J. Toole, and R. Woodgate

1) Circulation

In 2009, the annual wind-driven ocean circulation regime can be characterized as cyclonic (counterclockwise), with a Beaufort Gyre that is significantly reduced in strength and a Transpolar drift that is effectively nonexistent (Fig. 5.5). This is the first time that an annual cyclonic circulation regime has been observed in the Arctic since 1997. The anticyclonic circulation regime that persisted through 2008 lasted at least 12 years instead of the typical 5–8 year pattern [as reported in Proshutinsky and Johnson (1997), who analyzed statistics of Arctic circulation regimes between 1948 and 1989]. The climatological seasonal cycle of the Arctic has anticyclonic ice and ocean circulation prevailing in winter and cyclonic

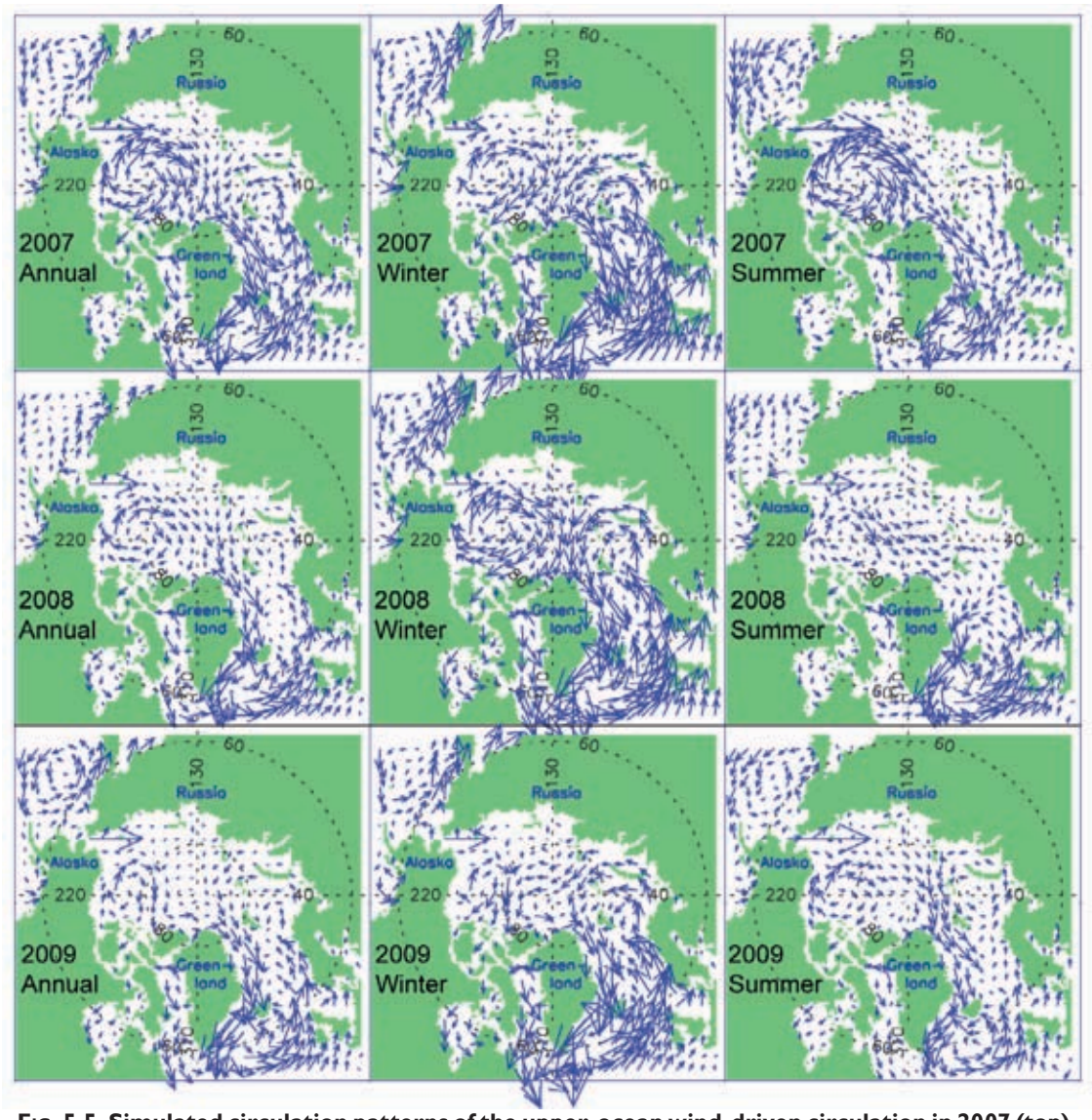

Fig. 5.5. Simulated circulation patterns of the upper-ocean wind-driven circulation in 2007 (top), 2008 (middle) and 2009 (bottom). Annual, winter, and summer circulations are shown in the left, center, and right panels, respectively.

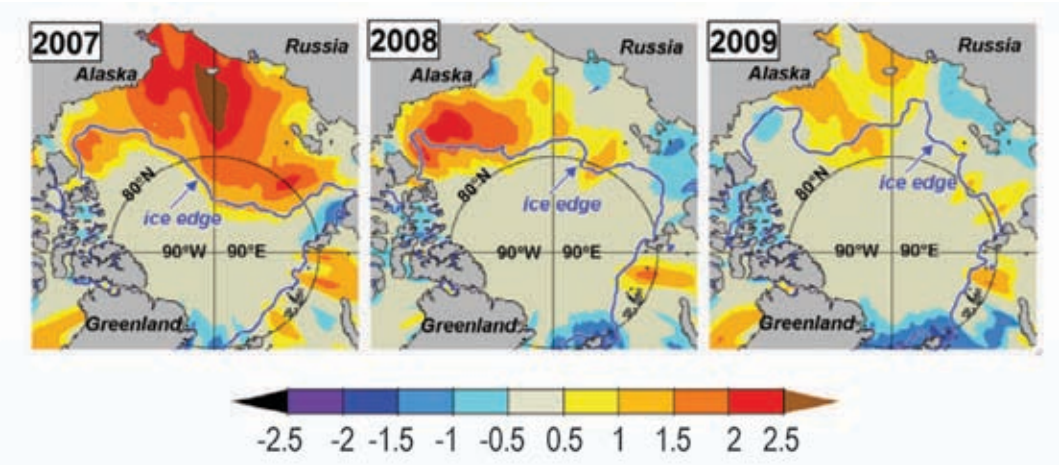

Fig. 5.6. Satellite-derived summer (JAS) SST anomalies (Reynolds et al. 2002) in 2007 (left), 2008 (middle), and 2009 (right) relative to the summer mean over 1982–2006. Also shown is the Sep mean ice edge (thick blue line).

circulation in summer. Since 2007, this seasonality has changed dramatically. In 2007, both summer and winter circulations were very strongly anticyclonic (Fig. 5.5, top panels) and resulted in the unprecedented reduction of the Arctic Ocean summer sea ice cover. In 2008, the winter circulation was anticyclonic but the summer circulation was unusual with a well-pronounced Beaufort Gyre and a cyclonic circulation cell north of the Laptev Sea (Fig. 5.5, middle panels). In 2009 (Fig. 5.5, bottom panels), the circulation reversed relative to climatology in both winter and summer: it was anticyclonic in summer (instead of cyclonic) and cyclonic in winter (instead of anticyclonic). These wind-driven conditions significantly influenced the characteristics of the sea ice cover, oceanic currents, ocean freshwater and heat content observed during 2007–09.

2) Water temperature and salinity

Maximum upper ocean temperatures in summer 2009 continued to decline since the historical extreme in summer 2007 (Fig. 5.6). This tendency is strongly linked to changes in the characteristics (e.g., pace and location) of the summer sea ice retreat and their effect on local atmospheric warming (Steele et al. 2010, manuscript submitted to *J. Geophys. Res.*). Surface warming and sea ice reduction in the Canada Basin has also been accompanied by the widespread appearance of a near-surface temperature maximum at 25–35 m depth due to penetrating solar radiation (Jackson et al. 2010). As described in the Arctic atmosphere section, the heat accumulated in the surface and near-surface layers of the ocean can be released back into the atmosphere in the fall—a cycle that is likely to influence sea ice conditions in the future.

Surface-layer waters in the Arctic Ocean in 2009 remained much fresher than in the 1970s (Timokhov and Tanis 1997, 1998). In the Beaufort Gyre, freshwater content in 2009 (Fig. 5.7) was comparable to the 2008 freshwater conditions, with the exception of the southwest corner of the Canada Basin. In this region, the freshwater accumulation was increased relative to 2008 by approximately 0.4 km^3 under enhanced Ekman pumping and sea ice melt in this region. In total, during 2003–09 the Beaufort Gyre (Proshutinsky et al. 2009) has accumulated approximately 5000 km^3 of freshwater (from 17 300 km^3 in 2003 to 22 300 km^3 in 2009), which is 5800 km^3 larger than climatology of the 1970s (Timokhov and Tanis 1997, 1998).

Hydrographic surveys conducted in 2007–09 summer (Fig. 5.7) in the Canada Basin indicate that in 2007 and 2008 there were two shallow temperature maximums in the upper Pacific water layer. However, in 2009, the heat content in this layer was reduced.

Atlantic Water layer maximum temperature anomalies for 2007–09 (Fig. 5.8) were calculated relative to the 1970s (Timokhov and Tanis 1997, 1998; Polyakov and Timokhov 1994). The 2007–09 Atlantic Water layer data were derived from ship-based and Ice-Tethered Profiler (ITP) instruments. In 2007–09, the temperature anomalies were generally higher on the Eurasian side of the Lomonosov Ridge, reaching a maximum of up to 1.5°C along the Eurasian Basin boundaries. Warming was less pronounced in the Canada Basin. There was little to no temperature anomaly (<0.1°C) at the southeast boundary of the Canada Basin or in the basin boundary regions adjacent to Greenland and the Canadian Archipelago. Negative (cooling) temperature anomalies were detected in the vicinity of Nares Strait. Considering 2009 data alone, the warming pattern remained similar with the major difference being that maximum temperature anomalies along the Eurasian Basin boundaries were lower (<1.0°C).

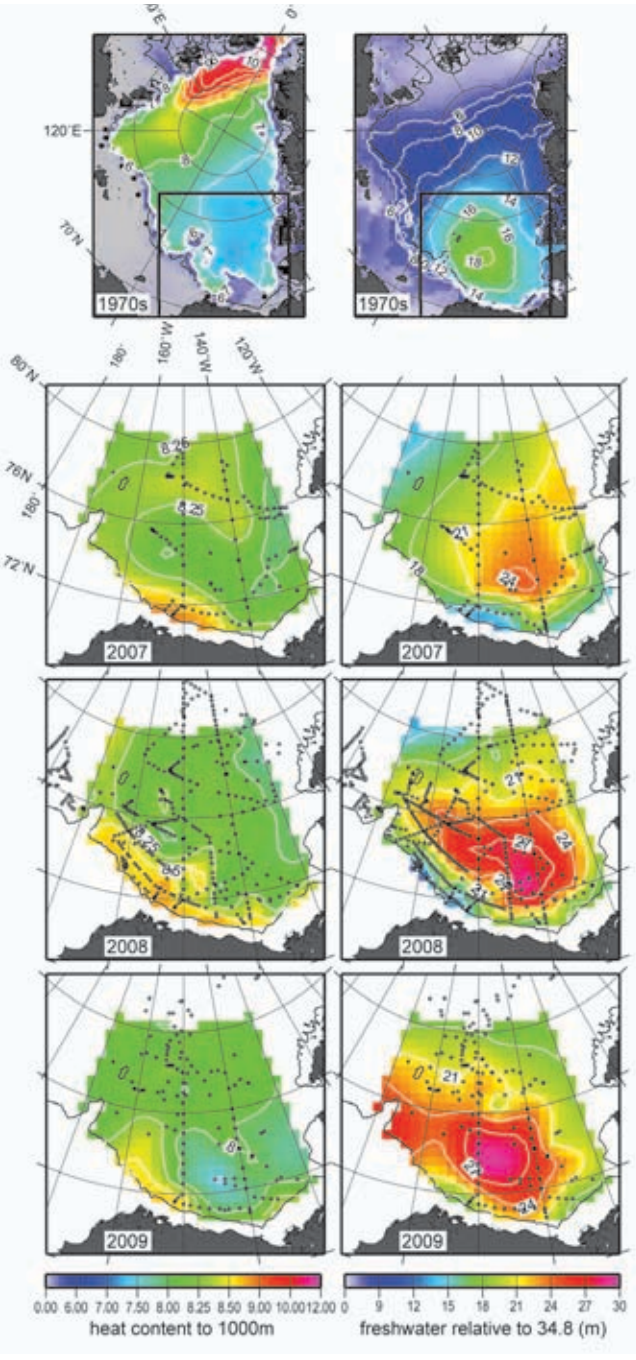

Fig. 5.7. Summer heat (1×10^{10} J m^{-2}) (left) and freshwater (m) content (right) in the 1970s, 2007, 2008, and 2009. The top two panels show heat and freshwater content in the Arctic Ocean based on 1970s climatology (Timokhov and Tanis 1997, 1998). The bottom six panels show heat and freshwater content in the Beaufort Gyre based on hydrographic surveys (black dots depict locations of hydrographic stations). For reference, this region is outlined in black in the top panel of each column. The heat content is calculated relative to water temperature freezing point in the upper 1000m ocean layer. The freshwater content is calculated relative to a reference salinity of 34.8.

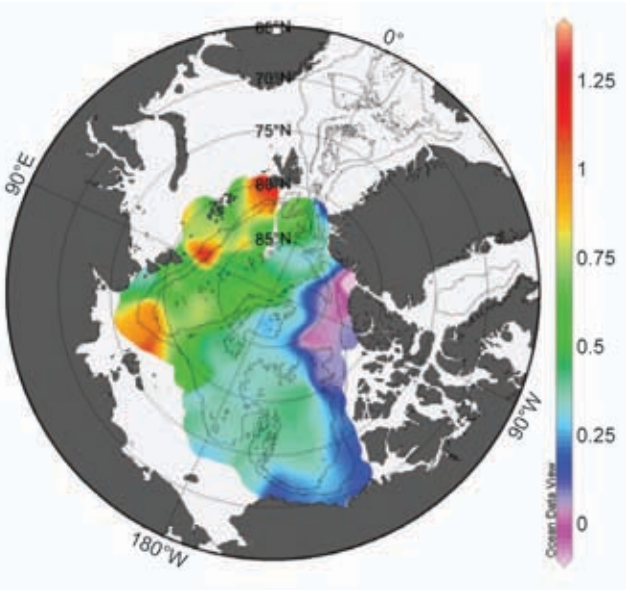

Fig. 5.8. 2007–09 Atlantic water layer temperature maximum anomalies relative to climatology of Timokhov and Tanis (1997, 1998).

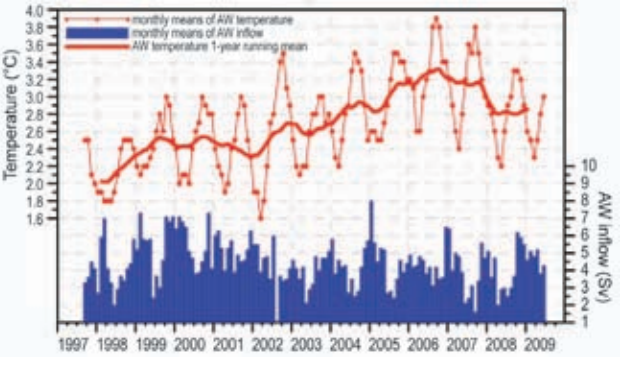

Fig. 5.9. Mean temperature of Atlantic water (AW, defined with TAW >1°C) and the AW volume inflow in the West Spitsbergen Current, northern Fram Strait measured by the array of moorings at 78°50'N.

The characteristics of the Atlantic Water layer discussed above are regulated by the Atlantic water parameters in the Fram Strait (Fig. 5.9), where the Atlantic water inflows to the Arctic Ocean. After reaching a maximum in 2006, the temperature of Atlantic water in Fram Strait decreased until 2008. In 2009, Atlantic water temperature and salinity in the northern Fram Strait started to rise again, returning to their long-term means. The late winter of 2008 and early spring of 2009 were also characterized by a higher Atlantic water volume inflow with the West Spitsbergen Current as compared to 2005–07 (Fig. 5.9).

The Bering Strait is another important gateway to the Arctic Ocean. Preliminary analysis of mooring data from the Bering Strait does not suggest a repeat

of the very high heat fluxes from 2007 (Woodgate et al. 2010). Temperatures in 2008 were generally cooler than in 2007, reaching only 2°C–3°C in near-bottom temperature, compared to 4°C–5°C in 2007. Similarly, by the time of mooring turnaround in 2009, water temperatures were about a degree colder than the same month (August) in 2007. These cooler temperatures are more in agreement with temperatures of 2000–06 in the strait.

An interesting change in ocean geochemistry was observed in the Canada Basin in 2008 and 2009. The input of sea ice meltwater, in combination with CO_2 uptake and global ocean acidification, caused the surface waters of the Canada Basin to become corrosive to calcifying organisms in the upper layer in 2008 (Yamamoto-Kawai et al. 2009). This is the first deep basin observation of aragonite undersaturation in surface waters. In 2009 the areal extent of surface waters unsaturated in aragonite, a form of calcium carbonate produced by marine organisms, increased. The increased stratification and decrease in upper-layer nutrient concentrations has also resulted in an increase in the number of picoplankton and a decrease in nanoplankton. Shifts such as these may alter the food web in the future (Li et al. 2009).

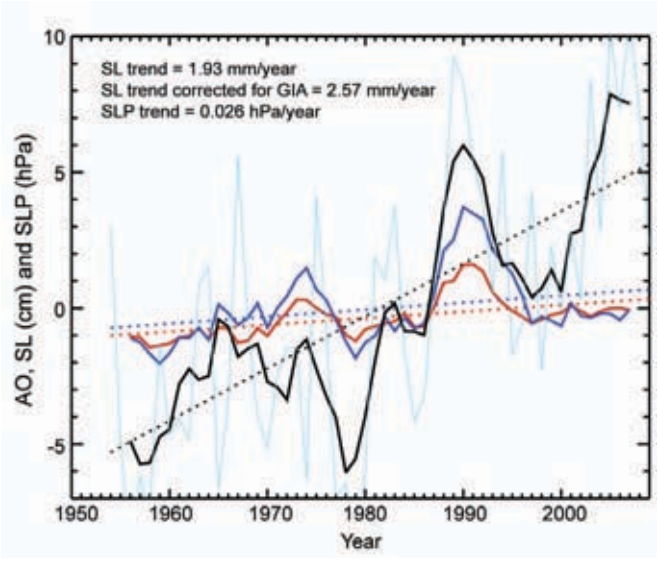

Fig. 5.10. Five-year running mean time series of: the annual mean sea level at nine tide gauge stations located along the Kara, Laptev, east Siberian, and Chukchi Seas' coastlines (black line); anomalies of the annual mean Arctic Oscillation (AO) Index multiplied by 3 (red line); sea surface atmospheric pressure at the North Pole (from NCAR–NCEP reanalysis data) multiplied by -1 (dark blue line); annual sea level variability (light blue line). Dotted lines depict estimated trends for SL, AO, and SLP.

3) Sea level

Fig. 5.10 shows sea level (SL) time series from nine coastal stations in the Siberian Seas, having representative records for the period of 1954–2009 (Arctic and Antarctic Research Institute data archives). In 2009, the SL along the Siberian coastline has significantly decreased relative to 2008. This caused a slight reduction in the estimated rate of SL rise for the nine stations over the period, to 2.57 ± 0.45 mm yr^{-1} (after correction for glacial isostatic adjustment, GIA). The changing SL rise tendency may be due to the substantial change in the wind-driven ocean circulation regime (less anticyclonic, as described in section 5c1) and/or due to steric effects associated with the reduction of surface ocean warming and freshening rates (section 5c2). Ocean cooling and salinification both result in sea level decrease.

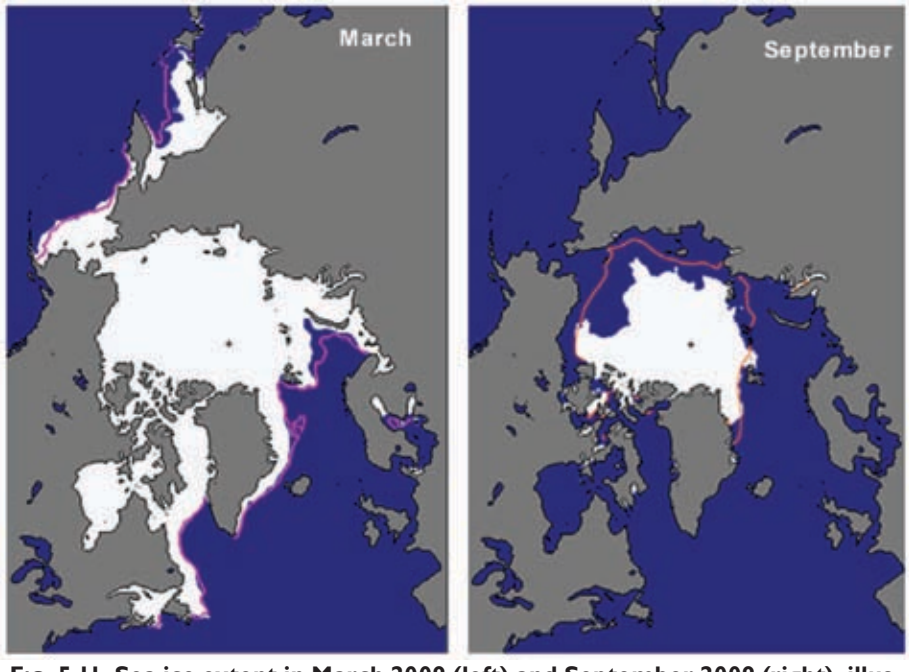

Fig. 5.11. Sea ice extent in March 2009 (left) and September 2009 (right), illustrating the respective winter maximum and summer minimum extents. The magenta line indicates the median maximum and minimum extent of the ice cover, for the period 1979–2000. (Source: National Snow and Ice Data Center.)

d. Sea ice cover—D. Perovich, R. Kwok, W. Meier, S. Nghiem, and J. Richter-Menge

1) Sea ice extent

Sea ice extent is the primary parameter for summarizing the state of the Arctic sea ice cover. Microwave satellites have routinely and accurately monitored the extent since 1979. There are two periods that define the annual cycle and thus are of particular interest: March, at the end of winter when the ice is at its maximum extent, and September, when it reaches its annual minimum. Ice coverage maps for March 2009 and September 2009 are presented in Fig. 5.11, with the magenta line denoting the median ice extent for the period 1979–2000.

The March 2009 maximum ice extent was 15.2 million km^2, the same as in 2008 and only 4% less that the 1979–2000 average of 15.8 million km^2. On 12 September 2009 sea ice extent reached a 2009 minimum of 5.1 million km^2. The 2009 summer minimum is the third-lowest recorded since 1979. It was 0.6 km^2 greater than 2008 and 1.0 km^2 above the record low in 2007 (an increase of 25% compared to 2007). Surface air temperatures through the 2009 summer were relatively cooler, particularly in the Chukchi and Beaufort seas. Winds in 2009 also tended to disperse the ice pack over a larger region. While the 2009 minimum extent was an increase over the two previous years, it was still 1.6 million km^2 (~10%) below the 1979 to 2000 average minimum. By December 2009 the ice extent had increased to 12.5 million km^2, the fourth lowest December extent on record. This relatively slow recovery was due in part to a strongly negative Arctic Oscillation in the fall, an atmospheric circulation pattern that promotes meridional flow and relatively warm air temperatures in the Arctic.

The time series of the anomalies in sea ice extent in March and September for the period 1979–2009 are plotted in Fig. 5.12. The anomalies are computed with respect to the average from 1979 to 2000. The large interannual variability in September ice extent is evident. Both winter and summer ice extent exhibit a negative trend, with values of -2.5% per decade for March and -8.9% per decade for September over the period 1979–2009.

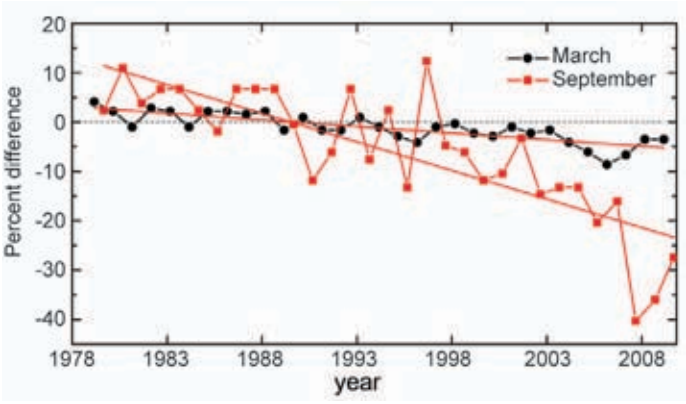

Fig. 5.12. Time series of the percent difference in ice extent in March (the month of ice extent maximum) and September (the month of ice extent minimum) relative to the mean values for the period 1979–2000. Based on a least squares linear regression for the period 1979–2009, the rate of decrease for the March and September ice extents is –2.5% and –8.9% per decade, respectively.

2) Sea ice age and thickness

The age of the sea ice is another key descriptor of the state of the sea ice cover, since older ice tends to be thicker and more resilient than younger ice. A simple two-stage approach classifies sea ice into first year and multiyear ice. First-year is ice that has not yet survived a summer melt season, while multiyear ice has survived at least one summer and can be several years old. Satellite derived maps of ice age for March of 2007, 2008, and 2009 are presented in Fig. 5.13.

In the past decade, the extent of multiyear sea ice rapidly reduced at a rate of 1.5×106 km^6 per decade, triple the reduction rate during the three previous decades (1970–2000). Springtime multiyear ice extent was the lowest in 2008 in the QuikSCAT data record since 2000 (Nghiem et al. 2007). QuikSCAT results in March 2009 showed a multiyear ice extent of 3.0 ± 0 .2 million km^2. This was 0.3 million km^2 larger

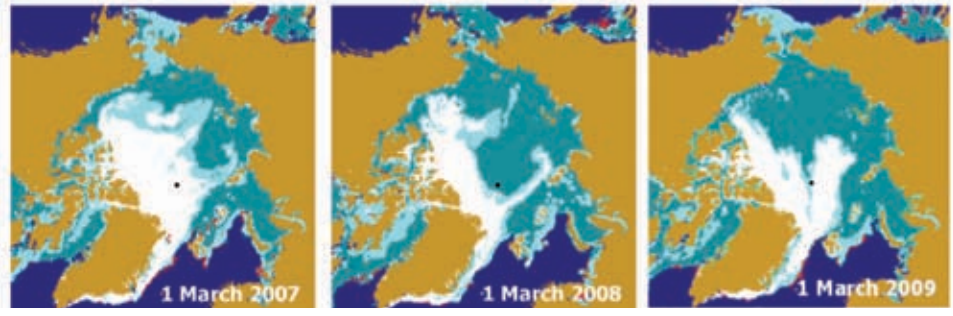

Fig. 5.13. Arctic sea ice distribution in March of 2007, 2008, and 2009. Multiyear ice is in white, mixed ice aqua, first-year ice teal, and ice with melting surface red. Dark blue is for open water and brown for land. Figure courtesy of Son Nghiem.

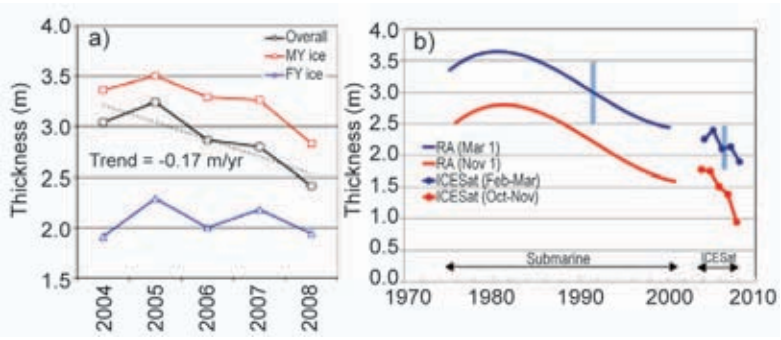

Fig. 5.14. (a) Winter Arctic Ocean sea ice thickness from ICESat (2004–08). The black line shows the average thickness of the ice cover while the red and blue lines show the average thickness in regions with predominantly multiyear and first-year ice, respectively. (b) Interannual changes in winter and summer ice thickness from the submarine and ICESat campaigns within the data release area for a period of more than 30 years. The data release area covers approximately 38% of the Arctic Ocean. Blue error bars show the uncertainties in the submarine and ICESat datasets (Kwok et al. 2009).

(11% increase) than the multiyear ice extent on the same date in 2008, even though the total sea ice extent was similar in the spring of 2008 and 2009. While the multiyear ice extent was similar in March 2008 and 2009, its distribution was quite different. More specifically, in 2008 there was a significant amount of multiyear ice in the Beaufort Sea and in 2009 there was a large amount of multiyear ice in the central Arctic Ocean.

Changes in ice age also have implications for the average ice thickness (Haas et al. 2008; Kwok 2007; Maslanik et al. 2007; Giles et al. 2008). Recent estimates of Arctic Ocean sea ice thickness from satellite altimetry show a remarkable overall thinning of ~0.6 m between 2004 and 2008 (Fig. 5.14a). Since the average thickness of the thinner first-year ice in midwinter (~2 m) did not exhibit a downward trend (blue line in Fig. 5.14a), the declines in total volume and average thickness (black line in Fig. 5.14a) are explained almost entirely by thinning and loss of multiyear sea ice due to melting and ice export. The total multiyear ice volume in the winter experienced a net loss of more than 40% in the four years since 2005 while the first year ice cover gained volume due to increased overall coverage of the Arctic Ocean. These changes have resulted in seasonal ice becoming the dominant Arctic sea ice type, both in terms of area coverage and of volume. In 2008, seasonal ice covered more than two-thirds of the Arctic Ocean.

In Fig. 5.14b the recent satellite estimates (ICESat) are compared with the longer historical record of declassified sonar measurements from U.S. Navy submarines (Kwok et al. 2009; Rothrock et al. 2008). Multiple regression of the submarine data was used to separate interannual changes, the annual cycle, and spatial changes. Within the submarine data release area (covering ~38% of the Arctic Ocean), the overall mean winter thickness of 3.6m in 1980 can be compared to a 1.9 m mean during the last winter of the ICESat record in 2008, a decrease of 1.7 m in thickness. This combined submarine and satellite record shows a long-term trend of sea ice thinning over submarine and ICESat records that span three decades.

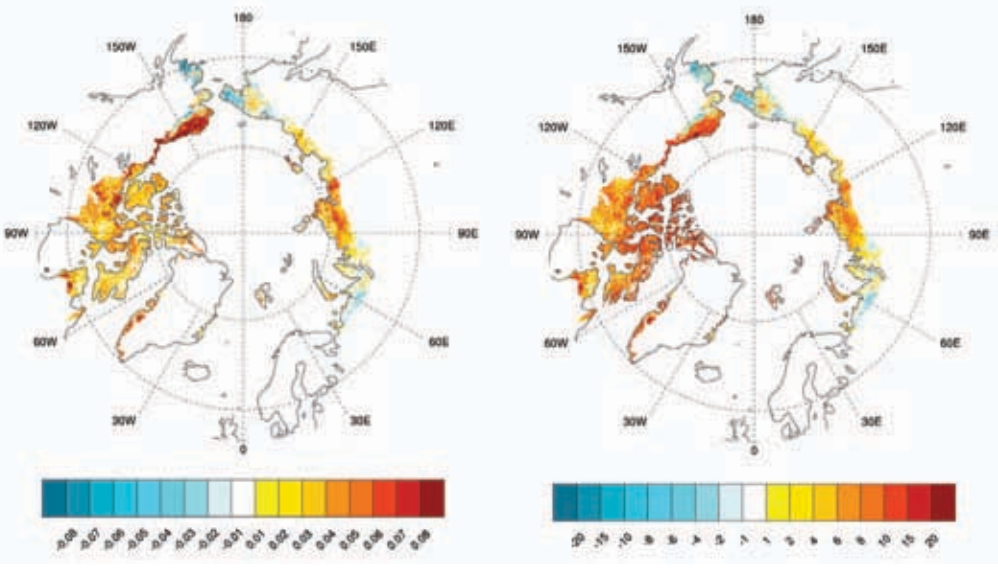

Fig. 5.15. Magnitude (unitless, left) and percentage (right) change of maximum NDVI from 1982 to 2008 for the circumpolar arctic tundra region. Colors show changes only within the area north of the Arctic tree line. Color scales are not linear (Bhatt et al. 2009, manuscript submitted to *Earth Interactions*).

e. *Land*

1) Vegetation—D. A. Walker, U. S. Bhatt, J. C. Comiso, H. E. Epstein, W. A. Gould, G. H. R. Henry, G. J. Jia, S. V. Kokelj, T. C. Lantz, J. A. Mercado-Díaz, J. E. Pinzon, M. K. Raynolds, G. R. Shaver, C. J. Tucker, C. E. Tweedie, and P. J. Webber

The summer greenness of Arctic tundra vegetation as measured using the maximum Normalized Difference Vegetation Index (MaxNDVI) has generally increased during the period 1982–2008 (Fig. 5.15). Changes in MaxNDVI are much greater in North America (9% increase) than Eurasia (2%). Coherent temporal relationships between near coastal sea ice, summer tundra land surface temperatures, and vegetation productivity have been demonstrated using Advanced Very High Resolution Radiometer (AVHRR)-derived 3g NDVI data (Pinzon et al. 2009, manuscript submitted to *EOS, Trans. Amer. Geophys. Union*; Bhatt et al. 2009, manuscript submitted to *Earth Interactions*). Absolute MaxNDVI changes are by far the greatest in the northern Alaska/Beaufort Sea area (0.09 AVHRR NDVI units), whereas the percentage changes have been highest in the Baffin Bay, Beaufort Sea, Canadian Archipelago, and Davis Strait areas (10–15% changes) (Fig. 5.15). The changes in NDVI are positively and significantly correlated with changes in summer Arctic land surface temperatures. Yearly variations in summer land temperatures are strongly and negatively correlated with yearly variations in the summer coastal sea ice (Bhatt et al. 2009, manuscript submitted to *Earth Interactions*). These observations support model projections that the Arctic land surfaces should warm as a result of the reduced summer extent of sea ice (Bhatt et al. 2008; Lawrence et al. 2008) and furthermore indicate that tundra ecosystems are responding to the increased summer warmth. Changes in the timing of tundra green up and senescence are also occurring. Green up is earlier in the cold sparsely vegetated high latitudes, whereas a shift to a longer green season is occurring during the fall in the more continuously vegetated southern Arctic (Jia et al. 2009). These changes are evident through the analysis of NOAA AVHRR satellite data in the Canadian Arctic for the period 1982–2003.

The greening trends observed in the satellite data are now supported by quantitative, long-term in situ vegetation measurements from the International Tundra Experiment (ITEX) and the Back to the Future (BTF) projects. As in the satellite measurements, the most evident changes appear to be occurring first in the sparsely vegetated areas of the far North. A study of plots at Alexandra Fiord, Ellesmere Island, is the first to demonstrate significant changes in above and below ground biomass over the last 25–30 years (Hill and Henry 2010; Hudson and Henry 2009) (Fig. 5.16). In addition, there has been a change in the relative abundance of species with an increase in the dominant species over this same time period. The changes in the tundra plant communities are most likely in response to the increase in temperature over the past 35 years of between 0.6°C–1.0°C per decade, with the strongest increases seen in the winter temperatures. The increases in biomass also correspond with longer growing seasons, with extensions into the late summer and with deeper active layers (depth of summer soil thawing). In another far-north Canada study, repeat photographs of permanent vegetation study plots 46 years after their initial installation near the Lewis Glacier, Baffin Island, document rapid vegetation changes along the margins of large retreating glaciers (Johnson et al. 2009b; P. J. Webber and C. E. Tweedie 2009, personal communication).

Further south, in the more lush tundra near Toolik Lake, a detailed analysis of a 20-year record (1989–2008) of tundra vegetation structure and composition from a set of 156 permanent monitoring plots indicates a general increase in above ground biomass (Gould and Mercado-Díaz 2008). Over the last two decades the relative abundance of vascular vegetation increased by 16%, while the relative abundance of nonvascular vegetation decreased by 18%. The canopy height, as well as the extent and complexity of the canopy have been increasing over time with the amount of horizontal surface having multiple strata increasing from about 60% to 80%.

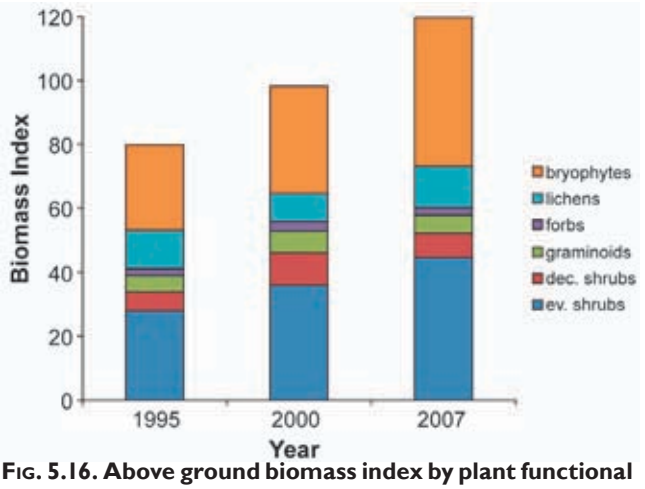

Fig. 5.16. Above ground biomass index by plant functional type for 18 permanent vegetation plots at Alexandra Fiord, Ellesmere Island, Canada, in 1995, 2000, and 2007. Values were the mean number of living tissue hits per plot using the point intercept method. Total live vegetation, bryophytes, and evergreen shrubs increased significantly over the period at p = 0.05. (Hudson and Henry 2009).

The frequencies of landslides, thermokarst features (irregular land surfaces formed in permafrost regions by melting ground ice), and fires have been noted in several areas of the Arctic (B. Jones et al. 2009; Kokelj et al. 2009; Lantz 2008; Lantz and Kokelj 2008; Walker et al. 2009; Leibman and Kizyakov 2007; Ukraientseva 2008). Warmer soil temperatures, melting permafrost, more abundant water, and increased nutrients on these features result in their pronounced greening.

In late summer 2007, the Anaktuvuk River fire near the University of Alaska's Toolik Lake Field Station burned almost 1000 km^2. It is the largest known fire to occur in northern Alaska and offered an opportunity for detailed analysis of the changes to the tundra energy and nutrient balance (Liljedahl et al. 2007) and spectral properties (Rocha and Shaver 2009). The burning itself released ~1.9 million metric tons of carbon to the atmosphere, which was about 30% of the carbon stock within the vegetation and active layer of this area (M. C. Mack, unpublished data).

2) Permafrost—V. Romanovsky, N. Oberman, D. Drozdov, G. Malkova, A. Kholodov, S. Marchenko

Observations show a general increase in permafrost temperatures during the last several decades in Alaska (Romanovsky et al. 2002; Romanovsky et al. 2007; Osterkamp 2008), northwest Canada (Couture et al. 2003; Smith et al. 2005), Siberia (Oberman and Mazhitova 2001; Oberman 2008; Drozdov et al. 2008; Romanovsky et al. 2008), and Northern Europe (Isaksen et al. 2000; Harris and Haeberli 2003).

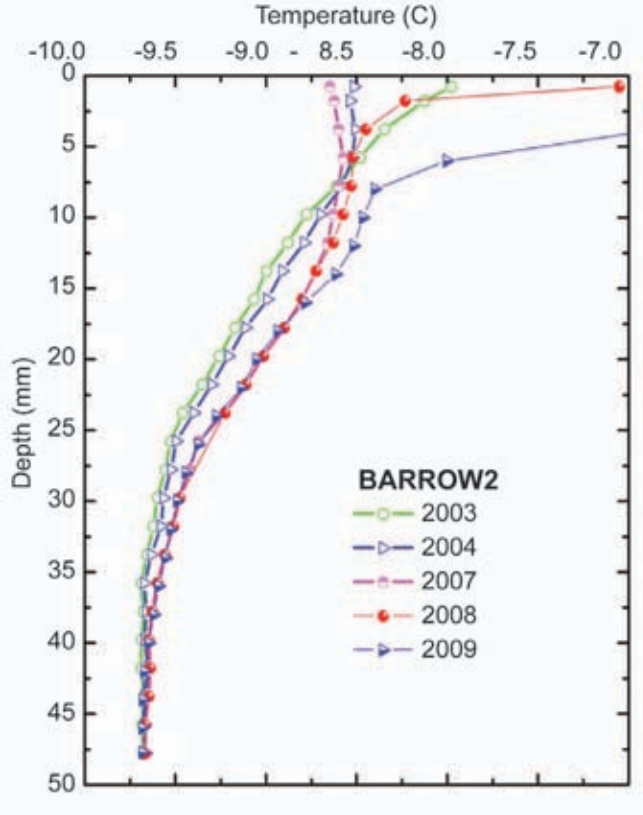

Fig. 5.17. Changes in permafrost temperature at different depths at the Barrow, Alaska, Permafrost Observatory in 2002–09.

Most of the permafrost observatories in Alaska show a substantial warming during the 1980s and 1990s. The detailed characteristic of the warming varies between locations but is typically from 0.5°C to 2°C at the depth of zero seasonal temperature variations in permafrost (Osterkamp 2008). However, during the last nine years, the permafrost temperature has been relatively stable on the North Slope of Alaska. There was even a slight decrease in the Alaskan Interior during the last three years. Only coastal sites in Alaska still show continuous warming, especially during the last three to four years (Fig. 5.17).

Permafrost temperature has increased by 1°C to 2°C in northern Russia during the last 30 to 35 years. A common feature for Alaskan and Russian sites is more significant warming in relatively cold permafrost than in warm permafrost in the same geographical area. An especially noticeable permafrost temperature increase in the Russian Arctic was observed during the last three years—the mean annual permafrost temperature at 15m depth increased by more than 0.35°C in the Tiksi area and by 0.3°C at 10m depth in the European North of Russia.

The last 30 years of increasing permafrost temperatures have resulted in the thawing of permafrost in areas of discontinuous permafrost in Russia (Oberman 2008). This is evidenced by changes in the depth and number of taliks (a layer of year-round unfrozen ground that lies in permafrost), especially in sandy and sandy loam sediments compared to clay. A massive development of new closed taliks in some areas of the continuous permafrost zone, as a result of increased snow cover and warming permafrost, was responsible for the observed northward movement of the boundary between continuous and discontinuous permafrost by several tens of kilometers (Oberman and Shesler 2009).

3) River discharge—A. Shiklomanov

Annual river discharge to the Arctic Ocean from the major Eurasian rivers in 2008 was 2078 km^3 (Fig. 5.18). In general, river discharge shows an increasing trend over 1936–2008 with an average rate of annual change of 2.9 ± 0.4 km^3 yr^{-1}. An especially intensive increase in river discharge to the ocean was observed during the last 20 years when the sea ice extent in the

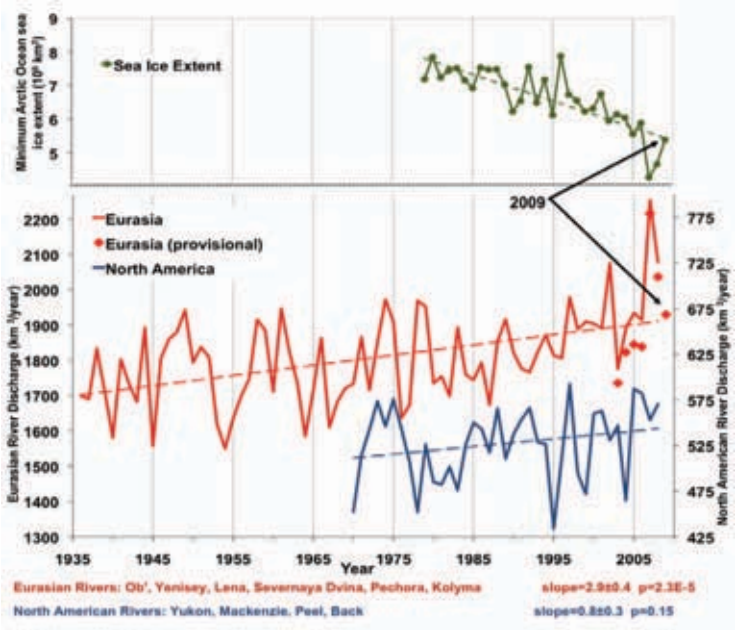

Fig. 5.18. Total annual river discharge to the Arctic Ocean from the six largest rivers in the Eurasian Arctic for the observational period 1936–2008 (updated from Peterson et al. 2002) (red line) and from the four large North American pan-Arctic rivers over 1970–2008 (blue line). The least squares linear trend lines are shown as dashed lines. Provisional estimates of annual discharge for the six major Eurasian Arctic rivers, based on near-real-time data from http://RIMS.unh.edu, are shown as red diamonds. Upper green line shows the September (minimum) sea ice extent in the Arctic Ocean over 1979–2009 from NSIDC (http://nsidc.org/data).

Arctic Ocean began decreasing. Interestingly, the correlation between Eurasian river discharge and sea ice extent over 1979–2008 is r = -0.72, or greater than the correlation between precipitation (Willmott et al. 1996) and runoff in these Eurasian drainage basins (r = 0.54). This suggests that both rivers and sea ice were responding to changes in large-scale hemispheric climate patterns (Shiklomanov and Lammers 2009). There is also an increasing tendency in river discharge to the Arctic Ocean from North America (Fig. 5.18) (Shiklomanov and Shiklomanov 2003; Rawlins et al. 2010). The mean annual discharge to the ocean over 2000–08 from the four large North American Arctic rivers was 6% (31 km^3) greater than the long-term mean from 1970–99.

Official river discharge data are usually processed and published with some delay. This gap is related to discharge calculation techniques that take into account diverse flow conditions and ambiguous relationships between measured water stage (water level) and estimated river discharge. Cold regions with long periods of ice cover present the most difficult conditions for reliable discharge estimates in near–real time (Shiklomanov et al. 2006). However, in cooperation with Russian partners, we developed a method to estimate river discharge from the most important Russian monitoring sites in near–real time using provisional stage measurements and river ice data (http://RIMS.unh.edu). Provisional estimates for the 2009 annual river discharge to the Arctic Ocean from the six Eurasian rivers was greater than the long-term mean over 1936–2008 but much smaller than discharge in 2007 and 2008 (Fig. 5.18). Taking into account that the provisional estimates over 2003–07 show a tendency to underestimate the annual observed values within an error of ± 2–4%, we anticipate the total discharge of six largest Eurasian rivers in 2009 being in the range 1930–1970 km^3.

4) Terrestrial snow—C. Derksen, R. Brown, and L. Wang

The 2008/09 Arctic snow cover season marked a continuation of the shorter snow seasons (due primarily to an early disappearance of snow cover in spring) observed during the last two decades following a rapid reduction in snow cover duration (SCD) that occurred in the 1980s.

Characterizing Arctic snow cover with conventional observations is a challenge because the station network is sparse, biased to coastal locations (particularly in North America), and the measurements themselves are uncertain. For instance, point snow depth measurements are subject to local scale wind drifting or scour and may not represent the prevailing regional conditions. Even when they do, the large distances between stations does not allow for meaningful spatial interpolation (i.e., kriging), and coastal stations do not represent vast inland areas. Because of these limitations, both satellite measurements and modeling approaches are necessary to characterize the various parameters related to Arctic snow cover, including snow cover extent (SCE), snow water equivalent (SWE), SCD, and snowmelt timing/duration.

For the 2008/09 snow season, analysis of the NOAA snow extent data record derived primarily from optical satellite imagery (http://climate.rutgers.edu/snowcover/) showed a shorter-than-normal snow cover season across a large portion of eastern Siberia, with strong negative anomalies in the North American sector confined to the Canadian

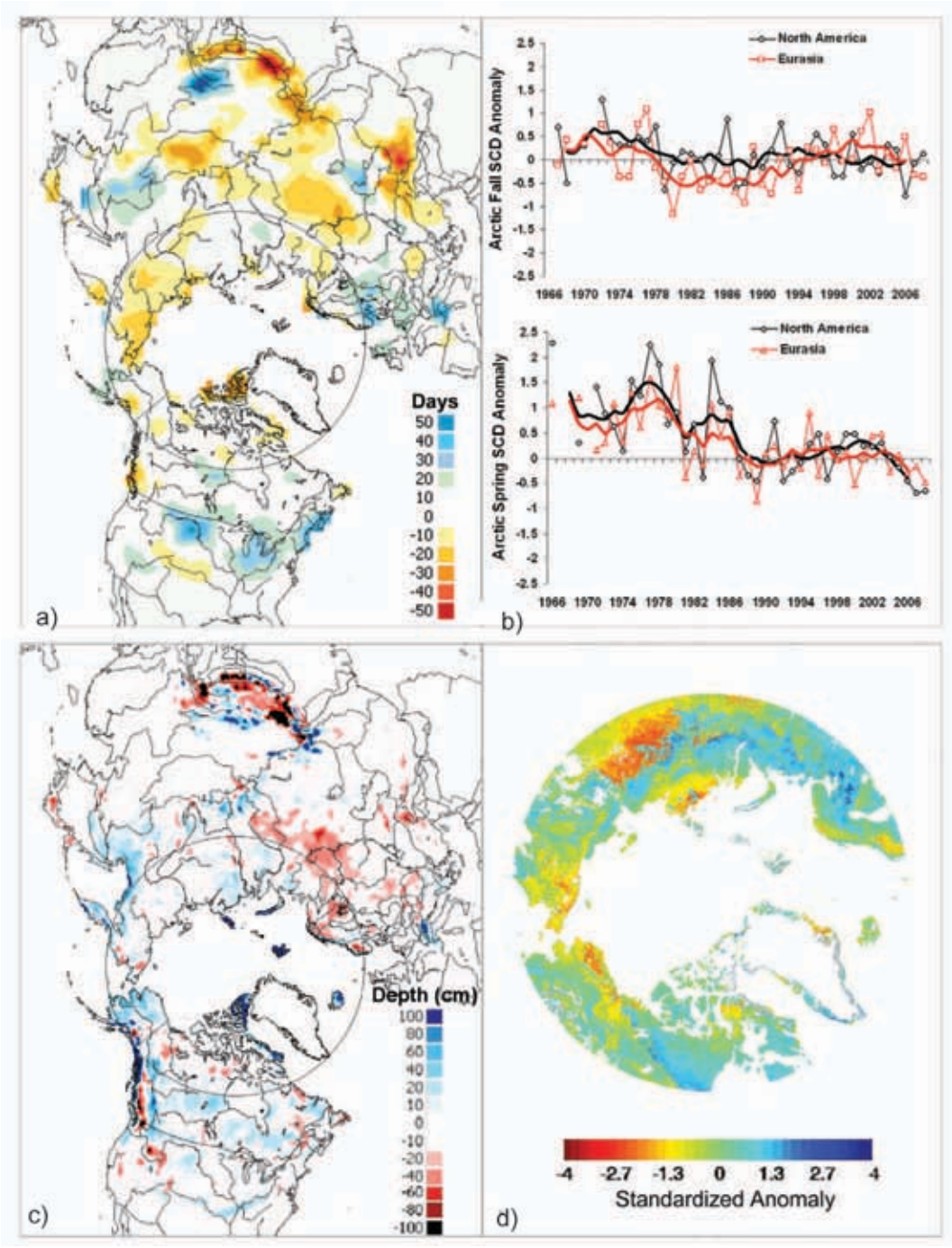

Fig. 5.19. (a) Snow cover duration (SCD) departures (with respect to 1988–2007) for the 2008/09 snow year and (b) Arctic seasonal SCD anomaly time series (with respect to 1988–2007) from the NOAA record for the first (fall) and second (spring) halves of the snow season. Solid lines denote 5-yr moving average; negative number means shorter snow season than normal. (c) Maximum seasonal snow depth anomaly for 2008/09 (with respect to 1998/99–2007/08) from the Canadian Meteorological Centre snow depth analysis. (d) Terrestrial snowmelt onset anomalies for 2009 (with respect to 2000–09) from QuikSCAT data derived using the algorithm of Wang et al. (2008).

Arctic Islands (Fig. 5.19a). The period 1988–2007 was selected as the historical reference period for these anomaly calculations to place the anomalies in the context of more recent snow cover conditions following a rapid reduction in hemispheric snow cover during the 1980s. When standardized SCD anomalies were calculated for NOAA grid cells north of 60°N and averaged for North America and Eurasia,

negative SCD anomalies were evident across Eurasia in the fall and the entire Arctic in spring (Fig. 5.19b). The shorter-than-average snow season in 2008/09 occurred in spite of slightly deeper-than-average snow depth (relative to the 1998–2009 average) in many parts of the Arctic (Fig. 5.19c), as identified by the daily global snow depth analysis (produced by combining the available ground observations with a snow model) from the Canadian Meteorological Centre (CMC, Brasnett 1999). Snowmelt onset anomalies determined from the QuikSCAT record (2000–09) derived with the algorithm of Wang et al. (2008) show that the initial timing of snowmelt in 2009 was near normal, or slightly later than normal across large regions of western Siberia, northern Europe, and the Canadian tundra (Fig. 5.19d). Collectively, these datasets suggest that although the snowpack was not anomalously shallow, and melt was initiated near the average time, the melt was of sufficient intensity to rapidly remove the snowpack across large regions of the Arctic. These observations are consistent with an intensification of snow-related high-latitude hydrological processes as discussed in Dery et al. (2009).

5) Glaciers outside Greenland—M. Sharp and G. Wolken (with data contributions from D. Burgess, J. G. Cogley, A. Arendt, and S. Luthcke)

Mountain glaciers and ice caps are a major contributor to global sea level change (Meier et al. 2007). In the Arctic ice masses of these types cover an area of over 400 000 km^2, representing 55% of the global glaciers and ice caps (excluding the ice sheets that cover Greenland and Antarctica). Although many of these glaciers lose mass by iceberg calving as well as by surface melt and runoff (Blaszczyk et al. 2009), the surface net mass balance (the difference between annual snow accumulation and annual runoff) is widely used as a measure of glacier response to climate variability and change. As measurements for the 2008/09 balance year are not yet available, we summarize measurements for 2007/08. These are available for 20 glaciers in Alaska (three), Arctic Canada (four), Iceland (nine) and Svalbard (four). Sixteen of the glaciers had a negative annual balance and four had a positive balance (two in Alaska and two in Svalbard). In addition, satellite gravimetry measurements reveal a regional annual net balance of -9 ± 20 Gt yr^{-1} for Gulf of Alaska glaciers. Here, two glaciers located close to the coast had positive annual balances, reflecting heavy winter snowfall in winter 2007/08, while Gulkana Glacier in the Alaska Range had a slightly negative annual balance. In Arctic Canada, annual net balances were among the three most negative balances recorded in the 43–48 year record, likely due to the very warm summer in 2008, extending the period of very negative balances that began in 1987. The annual balances recorded in Iceland were slightly more negative than average (16–17 years of record), while those in Svalbard were more positive than average (20–42 years of record).

Summer (JJA 2009) air temperature data (700 hPa level) and winter (September 2008–May 2009) precipitation data from the NCEP/NCAR Reanalysis provide indications of climatic conditions over the major glaciated regions of the Arctic in the 2008/09 mass balance year (Fig. 5.20; Table 5.1). Winter precipitation anomalies were positive (relative to the 1948–2008 mean) in Iceland and over the Alaska panhandle and adjacent areas to the north, and negative in southwest Alaska and southwest Svalbard. Summer temperature anomalies were strongly positive over southern Alaska, the Canadian Arctic and Svalbard, and very negative over Novaya Zemlya and Severnaya Zemlya.

Melt season duration, and the dates of melt onset and freeze-up, on Arctic glaciers and ice caps were determined from 2009 backscatter time-series measured by the SeaWinds scatterometer on QuikScat (Fig. 5.21; Table 5.1). In Arctic Canada, melt duration anomalies (relative to the 2000–04 average) were positive on all ice caps in the Queen Elizabeth Islands, with the largest anomalies occurring on the

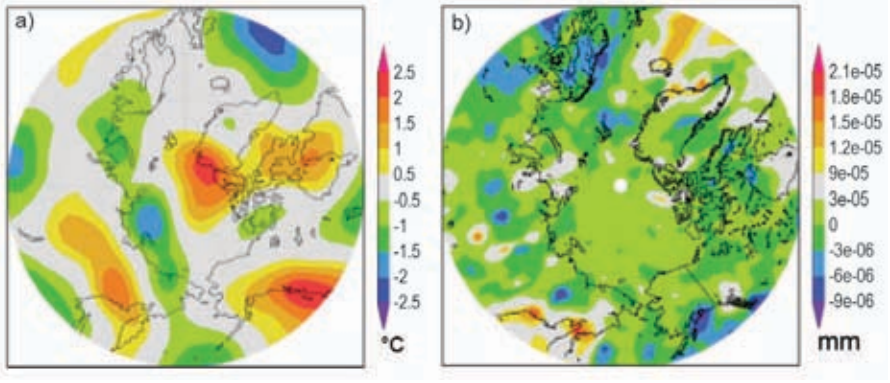

Fig. 5.20. Anomalies in (a) summer (JJA) 2009 air temperature (°C) at 700 hPa, and (b) winter (September 2008–May 2009) precipitation (mm) in the NCEP/NCAR Reanalysis relative to a 1948–2008 climatology.

Table 5.1. Summer (June–August) 2009 700 hPa air temperature and winter (September 2008–May 2009) precipitation anomalies (relative to 1948–2008 climatology from the NCEP/NCAR Reanalysis) for major glaciated regions of the Arctic (excluding Greenland). For ranks, 1 = year with highest summer temperature and winter precipitation. Anomalies in melt onset and freeze-up dates and summer melt duration (days) (relative to 2000–04 climatology) are derived from QuikScat V2 enhanced resolution scatterometer data. For melt season timing, negative anomalies indicate an earlier than normal date.

Region	Sub-Region	Latitude (N)	Longitude (E)	JJA 700hPa T Anomaly	2008 Rank	Sep-May Ppt Anomaly	2008 Rank	Melt Onset Anomaly	Freeze-up Anomaly	Melt Duration Anomaly
				(°C)	(/62)	(mm)	(/61)	days	days	days
Arctic Canda	N. Ellesmere Island	80.6 - 83.1	267.7 - 294.1	2.05	3	14.0	10	12.5	9.5	7.0
	Axel Heiberg Island	78.4 - 80.6	265.5 - 271.5	1.60	7	2/	4	6.2	5.7	9.0
	Agassiz Ice Cap	79.2 - 81.1	278.9 - 290.4	1.66	8	5.5	19	19.2	14.6	5.4
	Prince of Wales Icefield	77.3 - 79.1	278 - 284.9	1.16	11	10.6	13	7.3	5.7	3.8
	Sydkap	76.5 - 77.1	270.7 - 275.8	1.20	11	-39.2	49	4.5	3.8	2.0
	Manson Icefield	76.2 - 77.2	278.7 - 282.1	1.15	11	-51.7	51	-1.2	0.5	2.9
	Devon Ice Cap	74.5 - 75.8	273.4 - 280.3	0.90	16	-8	32	1.4	-2.0	4.7
	North Baffin	68 - 74	278 - 295	1.02	11	-0.9	25	1.1	-28.5	-9.9
	South Baffin	65 - 68	290 - 300	1.06	9	20.4	18	3.9	-12.6	-4.9
Eurasian Arctic	Severnaya Zemlya	76.25 - 81.25	88.75 - 111.25	-0.91	52	45.6	9	-2.3	29.3	-1.0
	Novaya Zemlya	68.75 - 78.75	48.75 - 71.25	-0.94	50	34.1	15	19.65	-12.9	-8.4
	Franz Josef Land	80 - 83	45 - 65	0.10	30	30.1	14	4.7	-8.9	-4.2
	Svalbard	76.25 - 81.25	8.75 - 31.25	0.46	18	-49.2	47	4.5	3.8	2.0
	Iceland	63 - 66	338 - 346	-0.09	37	258.6	3	2.7	14.6	-1.2
Alaska	SW Alaska	60 - 65	210 - 220	391.77	2	29.1	25	-10.7	3.0	0.1
	SE Alaska	55 - 60	220 - 230	1.92	3	167.4	9	*	*	*

northernmost ice caps (N Ellesemere, Agassiz, and Axel Heiberg) despite later-than-average melt onset dates. Melt duration anomalies were also positive on Svalbard and slightly positive in southwest Alaska, mainly due to both early melt onset and late freeze-up in the eastern Alaska Range. Melt duration anomalies were strongly negative on north and south Baffin Island, due to very negative (early) freeze-up anomalies,

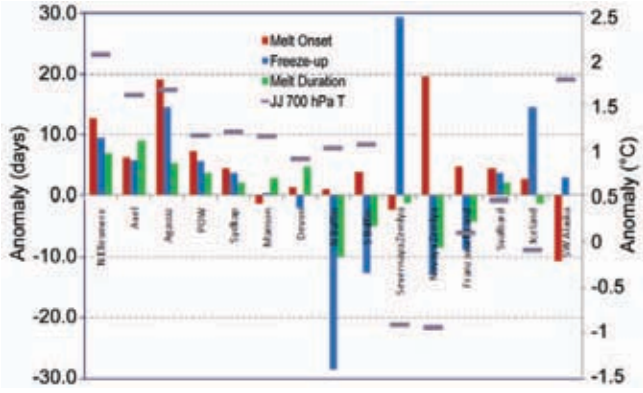

Fig. 5.21. Anomalies (relative to 2000–2004 climatology) in melt season duration and the dates of melt onset and freeze-up on Arctic glaciers and ice caps (outside of Greenland) derived from SeaWinds scatterometer on QuikScat, and anomalies in summer (JJA) 2009 air temperature (°C) at 700 hPa in the NCEP/NCAR Reanalysis relative to a 1948–2008 climatology. Melt onset and freeze-up dates define the first and last days on which melt occurred during the year. As there can be cold periods during the summer when melt ceases, the melt duration can be less than the number of days between the onset and freeze-up dates.

and on Novaya Zemlya, due to both very positive (late) melt onset and negative (early) freeze-up anomalies. Melt duration anomalies were also negative on Iceland and Franz Josef Land, and slightly negative on Severnaya Zemlya despite exceptionally positive (late) freeze-up anomalies.

By comparing 2009 summer temperature, winter precipitation, and melt season anomaly patterns with both the anomaly patterns and measured mass balances for 2007/08, we predict another very negative mass balance year in Arctic Canada (but probably not as negative as 2007/08), and annual balances more negative than in 2007/08 in Alaska, Svalbard and Franz Josef Land, and more positive than in 2007/08 in Iceland, Novaya Zemlya and Severnaya Zemlya.

f. Greenland—J. E. Box, I. Bhattacharya, J. Cappelen, D. Decker, X. Fettweis, K. Jezek, T. Mote, and M. Tedesco

1) Coastal surface air temperatures

Warmer-than-normal winter and summer air temperatures prevailed along the northwest Greenland coast in 2009, compared to the 1971–2000 average, according to surface air temperature data recorded at operational meteorological stations (Table 5.2). Summer air temperatures at Thule AFB/Pituffik were the warmest on record since 1961. Aasiaat summer temperatures were second warmest on record since 1950. At stations with records beginning in 1873, the only outstanding anomaly was summer at Upernavik ranking second warmest. In contrast, autumn surface temperatures anomalies along west Greenland were relatively cool.

2) Upper-air temperatures

Seasonally-averaged 2009 upper-air temperature data, available from twice-daily balloon sounds at the Integrated Global Radiosonde Archive (http://www.ncdc.noaa.gov/oa/climate/igra/) (Durre et al. 2006), indicate a pattern of warm atmospheric anomalies below ~5 km (Fig. 5.22). This is consistent with a warming trend prevailing since reliable records began in 1964 and especially since the mid-1980s (Box and Cohen 2006). A number of sites were outstanding. These included Danmarkshavn and Illoqqortoormiut, with record-setting warm anomalies in the winter in the lower stratospheric between 50 and 200 hPa, and Aasiaat, where the summer was the warmest on record since 1964 at 1000 hPa. The averaged total column (1000 hPa–20 hPa) temperatures in winter ranged between the fourth and second warmest on

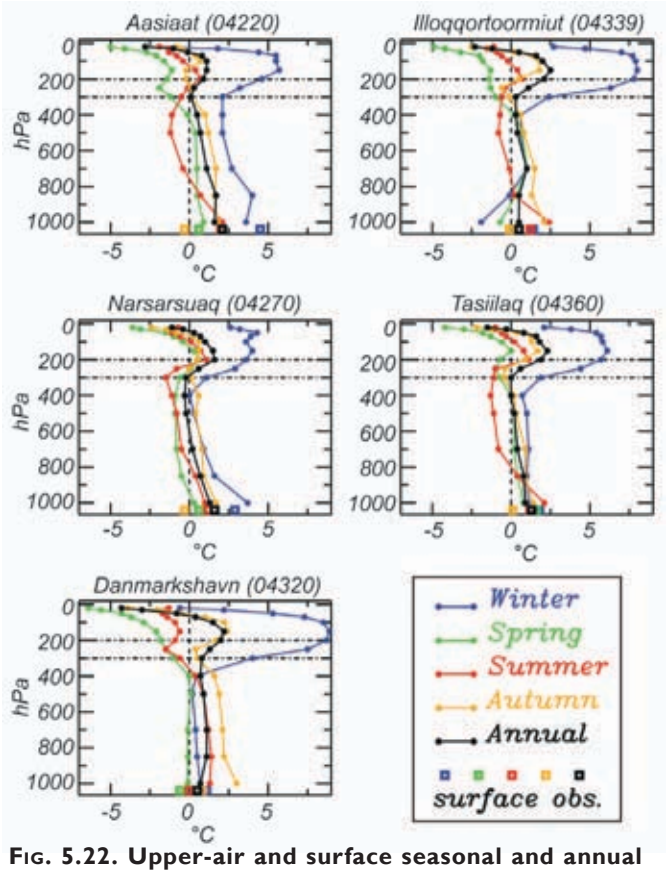

Fig. 5.22. Upper-air and surface seasonal and annual mean temperature anomalies in 2009, with respect to the 1971–2000 average. The station WMO ID number is indicated beside the location name. See Table 5.2 for site coordinates.

Table 5.2. 2009 Greenland station surface air temperature anomalies by season, relative to 1971–2000.

Station (Region) Latitude, Longitude, time range	Winter	Spring	Summer	Autumn	Annual
Thule AFB/Pituffik, 76.5 N. 68.8 W, 1961-2009	**3.7**	1.0	**2.6***	-1.4	**1.6**
Upernavik (NW), 72.8N, 56.2 W 1958-2009	**5.1**	1.0	**2.7**	0.9	**2.3**
Aasiaat (W), 68.7N 52.8, 1958-2009	**4.5**	0.6	**2.0**	0.3	2.1
Nuuk (SW), 64.2 N, 43.2 W, 1958-2009	2.3	0.1	1.1	**-0.6**	1.1
Prins Christian Sund (S), 60.0 N, 43.2 W, 1958-2009	1.4	0.6	0.7	0.4	1.0
Tasiilaq (SE) 65.6 N, 22.0 W, 1958-2009	1.8	1.6	**1.2**	0.1	**1.3**
Illoqqortoormiut (E), 70.4 N, 22.0 W, 1958-2009	1.4	0.1	1.2	-0.1	0.5
Danmarkshavn (NE), 76.8N 18.8 W, 1958-2009	1.1	0.6	0.0	0.8	0.5

*Anomalies are in °C, with respect to the 1971–2000 base period. Bold values indicate values that meet or exceed 1 standard deviation from the mean. Underlined values exceed 2 standard deviations from the mean. The * symbol indicates a record setting year. The winter value takes December from the previous year.

record among the sampling sites. In the spring, these sites were among the second/third coolest, making the annual total column mean temperature near normal. Surface air temperature anomalies (Table 5.2) are broadly consistent with the lowest level of the upper-air observations. The main exception is a consistent pattern of surface observations indicating a cool autumn season, while the lowest upper-air level (1000 hPa) indicates warming.

3) Atmospheric circulation anomalies

Persistent 500 hPa geopotential height anomalies drew more warm air than normal across northern Greenland (Fig. 5.23, see also Fig. 5.3). The pattern was very similar to that of 2008 (Fettweis et al. 2010). Consistent with the geopotential height anomaly, passive microwave satellite data indicate a higher number of melting days than normal at the north of the ice sheet and along the eastern margin.

4) Surface melt extent and duration

Passive microwave measures of melt extent (Mote 2007) indicate that the seasonally-averaged melt extent (JJA) in 2009 was near the 1979–2009 average and was also the lowest since 1996 (Fig. 5.24). There was less-extensive-than-average melt from mid-June through the first week of July and much more extensive-than-average melt during the remainder of July. August was near normal. Late June corresponded to periods of temperatures at 850 hPa averaging 1°C–3°C below normal over most of the ice sheet in the North American Regional Reanalysis, while 850 hPa temperatures were above normal during July across the northern half of the ice sheet. Passive (SMMR and SSM/I, 1979–2009) and active

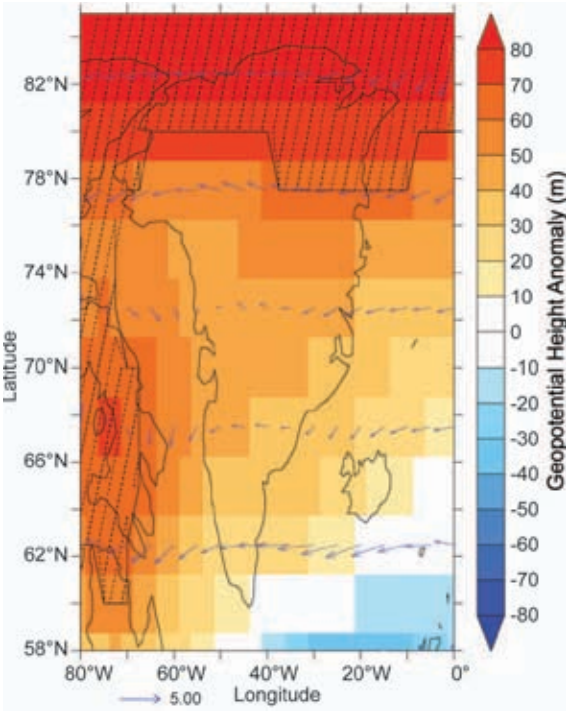

Fig. 5.23. The geopotential height and wind anomalies for JJA 2009 (referenced to the 1960–2009 mean) at 500 hPa from the NCEP/NCAR Reanalysis. Areas where geopotential height anomalies were at least twice the 1960–2009 standard deviation are hatched. The blue arrows represent wind vector anomalies, with scale indicated by the blue arrow below the plot

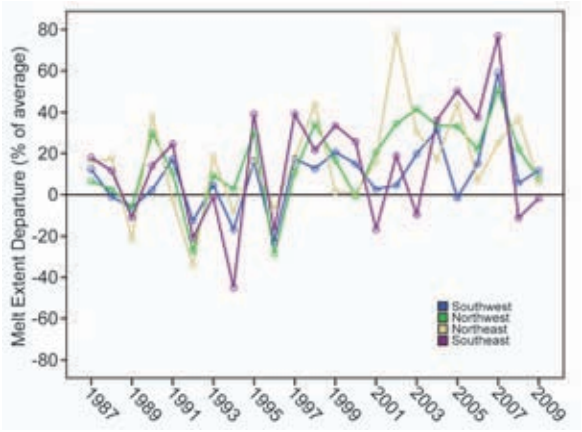

Fig. 5.24. Time series of Greenland regional melt extent anomalies derived from passive microwave remote sensing, after Mote (2007).

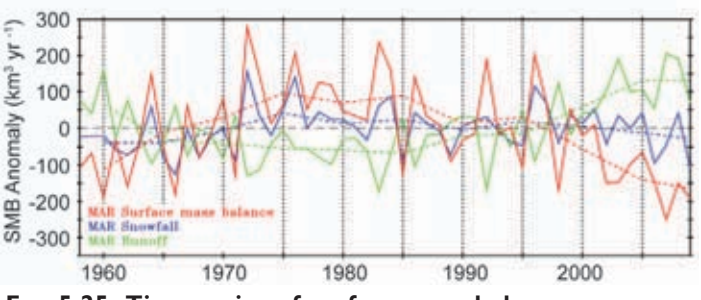

Fig. 5.25. Time series of surface mass balance component anomalies simulated by the regional climate MAR model (Fettweis et al. 2010).

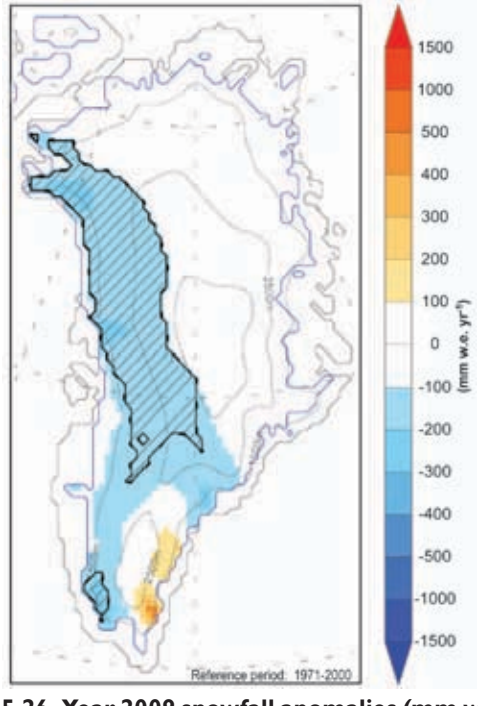

Fig. 5.26. Year 2009 snowfall anomalies (mm w.e. yr^{-1}) simulated by the regional climate MAR model (Fettweis et al. 2010). Hatched areas indicate an anomaly that is twice or more the 1971–2000 standard deviation.

(QuikSCAT, 2000–09) microwave remote sensing indicate substantially less melt duration in areas below ~1800 m elevation compared to recent years of high melt duration. More melting than normal is evident above ~800 m elevation in the north and eastern ice sheet.

5) Precipitation and surface mass balance

The balance between ice mass gain from snowfall and the loss from meltwater runoff is positive for any healthy ice mass. The 2009 surface mass balance anomaly was 25% to 50% less positive than normal (Fig. 5.25). This condition usually reflects a heavy melt year. However, in 2009 melt was below-normal (Table 5.3). The source of the relatively low surface mass balance was the below normal snow accumulation for Greenland, especially evident along the western slope (Fig. 5.26). For the ice sheet as a whole snowfall was 25% (150 Gt) below normal, resulting in below normal mass input to the ice sheet. The temperature and precipitation anomalies are very likely the result of regional circulation anomalies that deserve more attention.

6) North water polynya

Nares Strait, separating Greenland from Ellesmere Island is host to the largest recurring polynya (a persistent area of open water surrounded by sea ice) in the Arctic. This "North Water" polynya is formed by some combination of ocean heat and winds. Ecologically, the North Water is known to be a wildlife "bonanza" for marine mammals, including narwhal and beluga whales. Strong winds and large atmosphere-to-surface temperature contrast result in tremendous ocean-to-atmosphere heat transfer, frazil ice, and saline deep water production. The sea ice consolidated into land-fast ice 500 km north of its typical position (Fig. 5.27) in the Lincoln Sea, far enough outside of the mouth of Nares St. that the normal strong winds that funnel through the strait (Samelson et al. 2006; Samelson and Barber 2008) allowed an "ice bridge" to persist all winter and into summer 2009. Nares Strait remained unconsolidated the entire 2008/09 winter. On 7 July 2009, the ice bridge collapsed allowing the normal flow of Arctic Ocean pack ice into the strait that makes ship navigation normally difficult, even for ice breakers. Summer (JJA)-averaged MODIS-derived (MOD28 4.88 km) sea surface temperatures were nearly 2°C warmer in Kane Basin than the 2000–07 average. Passive microwave sea ice concentration indicates

Table 5.3. Greenland ice sheet surface mass balance anomalies, after Fettweis et al. (2010).

2009 anomaly referenced to	Toptal SMB (Gt)	Total Snowfall (Gt)	Total Runoff (Gt)	JJA Air Temperature (°C)
1971-2000	-280	-150	110	0.72
1991-2000	-230	-140	84	0.52
2001-2009	-85	-100	-37	-0.71

an unprecedented low sea ice concentration in Nares Strait during summer 2009, relative to the 1979–2009 average. AMSR-E 12.5 km passive microwave sea ice concentrations were 20% below the 2002–07 base average north of Smith Sound.

7) Outlet glaciers

Daily surveys of Greenland ice sheet marine-terminating outlet glaciers from cloud-free Moderate Resolution Imaging Spectroradiometer (MODIS) visible imagery (http://bprc.osu.edu/MODIS/) indicate that the 34 widest glaciers collectively lost 101 km^2 of marine-terminating ice between the end of summer 2008 and the end of summer 2009. Twenty-three of thirty-four of the glaciers retreated in 2009 relative to their end of summer 2008 position. The total net effective length change of these glaciers was -1.2 km. The largest area changes included a 32 km^2 loss along the 110 km wide Humboldt Glacier; a 31 km^2 loss at the calving front of another north Greenland outlet, the Zachariæ Isstrøm; and 15 km^2 ice loss at the Midgard glacier. This marked a continuation of a highly linear (R = -0.99) deglaciation trend (-104 km^2 yr^{-1}, Fig. 5.28) of the past 10 summers when MODIS data are available. The cumulative area change from end of summer 2000 to 2009 is -967 km^2, an area loss equivalent to 11 times the area of Manhattan Island.

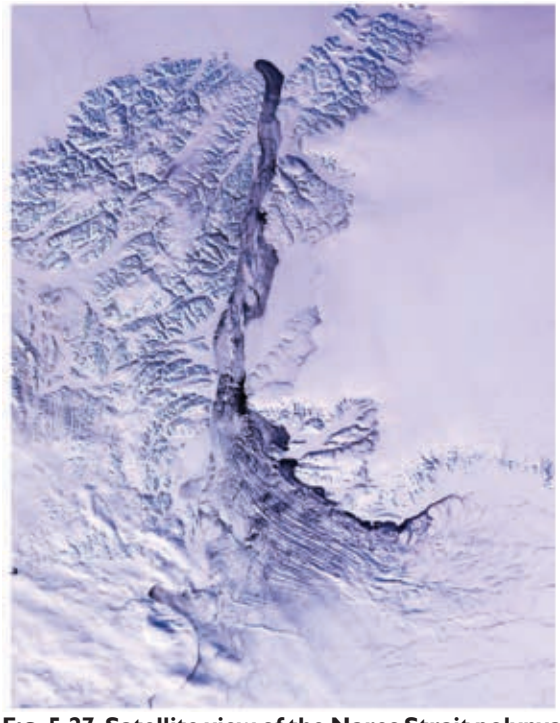

Fig. 5.27. Satellite view of the Nares Strait polynya between Arctic Canada and northwest Greenland. Note the wind-driven "sea smoke" cloud streaks, that is, ice fog condensate from the much warmer ocean surface.

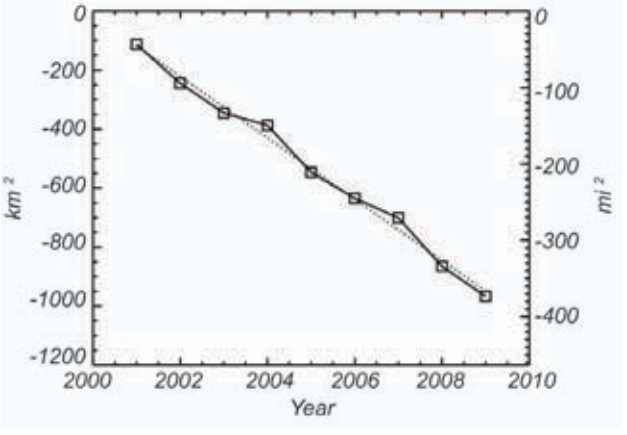

Fig. 5.28. Cumulative annual area changes for 34 of the widest Greenland ice sheet marine-terminating outlets.